
NIMMGen: Learning Neural-Integrated Mechanistic Digital Twins with LLMs

Zihan Guan^{*1} Rituparna Datta^{*1} Mengxuan Hu¹ Shunshun Liu¹ Aiying Zhang¹ Prasanna Balachandran¹
Sheng Li¹ Anil Vullikanti¹

Abstract

Mechanistic models encode scientific knowledge about dynamical systems and are widely used in downstream scientific and policy applications. Recent work has explored LLM-based agentic frameworks to automatically construct mechanistic models from data; however, existing problem settings substantially oversimplify real-world conditions, leaving it unclear whether LLM-generated mechanistic models are reliable in practice. To address this gap, we introduce the Neural-Integrated Mechanistic Modeling (NIMM) evaluation framework, which evaluates LLM-generated mechanistic models under realistic settings with partial observations and diversified task objectives. Our evaluation reveals fundamental challenges in current baselines, ranging from model effectiveness to code-level correctness. Motivated by these findings, we design NIMMgen, an agentic framework for neural-integrated mechanistic modeling that enhances code correctness and practical validity through iterative refinement. Experiments across three datasets from diversified scientific domains demonstrate its strong performance. We also show that the learned mechanistic models support counterfactual intervention simulation.

1. Introduction

Purely data-driven methods are inadequate for many fundamental problems associated with such complex systems, and integration with knowledge-guided or model-based methods is necessary, e.g., (Karpatne et al., 2022; Karniadakis et al., 2021). Digital Twins (DTs), which are data-driven computational and mechanistic models constructed based on domain knowledge from physical, biological or chemical processes, and are often tightly coupled with real-world dynamic systems, provide a very powerful framework for representing such systems, e.g., (National Academies of

Sciences, Engineering, and Medicine, 2023; Niederer et al., 2021; Holt et al., 2024). They are popular in various scientific domains, such as medicine (Marchal, 2025; Katsoulakis et al., 2024), power distribution (Meyur et al., 2022; Thorve et al., 2023), and computational epidemiology (Adiga et al., 2018; Marathe & Vullikanti, 2013; Cui et al., 2025; Chopra et al., 2022), and have been used for monitoring, simulation, and prediction of such systems. Hybrid models, which integrate neural networks and digital twins, have been shown to achieve better performance in many applications, e.g., (Cui et al., 2025; Holt et al., 2024).

Despite their practical value, constructing accurate mechanistic models is challenging. Motivated by recent advances in large language models (LLMs) for code generation and agentic optimization (Novikov et al., 2025; Tang et al., 2024; White et al., 2023), a growing line of work, such as HDTwinGen (Holt et al., 2024), has begun to explore LLM-driven frameworks that learn and refine mechanistic models directly from data. However, to deploy these LLM-driven frameworks for real-world usage, a fundamental challenge remains underexplored: *Are current LLM-based systems truly ready to generate mechanistic models for real-world scientific applications?* The existing evaluation environment in HDTwinGen relies on simplified assumptions of the real-world scenarios. Specifically, ❶ HDTwinGen setup considers full observation of the system states, whereas real-world scientific datasets are often only partially observed. Besides, ❷ their evaluation only focuses on the modeling task of the digital twin models, while ignoring other diversified tasks. Finally, ❸ the generated hybrid digital twin models are confined to the form of an additive combination of the neural network and the mechanistic component. More discussions are provided in § 3.1.

To address these limitations, we introduce the *Neural-Integrated Mechanistic Modeling* (NIMM) evaluation framework, which introduces **a new problem setting** for evaluating LLM-driven mechanistic model construction in scientific domains. Specifically, for point ❶, each dataset in NIMM provides only partial observations of the underlying system states; for example, in epidemiological datasets, only reported infection counts are observed, while latent compartments such as susceptible or exposed populations remain unobserved. For point ❷, the task objective in NIMM ex-

^{*}Equal contribution ¹University of Virginia. Correspondence to: Anil Vullikanti <vsakumar@virginia.edu>.

tends beyond fitting observed trajectories and encompasses datasets from three different domains with diverse tasks, including public health, clinical health, and materials science. Finally, for point ③, NIMM adopts a more general neural-integrated formulation inspired by recent advances in mechanistic modeling, with the hybrid digital twin model used in prior work as a special case. We evaluate the baselines across black-box neural networks, existing mechanistic models in the prior work, and the LLM-driven approaches over the NIMM evaluation framework. The evaluation results suggest that (1) existing baselines continue to struggle under the more challenging settings introduced by NIMM; (2) LLM-based approaches frequently have code-level errors when generating the complex neural-integrated mechanistic models; and (3) LLMs may produce models that are mathematically valid yet semantically incorrect.

Guided by these findings, we propose NIMMGen, an agentic framework for neural-integrated mechanistic modeling. The NIMMGen introduces a self-evolving optimization loop composed of a modeling agent and a reflection agent, which iteratively refines model specifications. To reduce code error rates, NIMMGen incorporates an error-correction module that augments the agent’s memory with historical error messages to reduce repeated failures. To filter out the models that are semantically incorrect, NIMMGen also incorporates a verification agent that evaluates the physical and semantic consistency of generated models. Across the three domains in the NIMM evaluation framework, our approach achieves strong empirical performance. Beyond effectiveness, we demonstrate that the learned mechanistic models can support counterfactual intervention simulation (e.g., social distancing), highlighting their utility for decision-relevant analyses. Our further analysis on the optimization process of the NIMMGen also suggests that NIMMGen progressively introduces substantive model changes that enable better adaptation to the environment.

In summary, this paper makes three contributions:

1. Novel Problem setting. We introduce NIMM, an evaluation framework that formalizes a *realistic problem setting* for LLM-based neural-integrated mechanistic modeling under partial observation and forecasting objectives, which are largely underexplored in prior work.

2. Effective Agentic Method. We propose NIMMGen, an agentic framework that learns effective neural-integrated models by explicitly targeting code-level correctness and semantical correctness during iterative model generation.

3. Empirical Evidence of Scientific Utility. We show that NIMMGen produces mechanistic models that achieve strong performance across three domains and enable counterfactual intervention simulation, demonstrating practical value.

2. Background

Let $\mathcal{S} := (\mathcal{X}, \mathcal{U}, \Phi)$ denote a dynamical system, which consists of $d_{\mathcal{X}}$ -dimensional states from its state space $\mathcal{X} \subseteq \mathbb{R}^{d_{\mathcal{X}}}$, the (optional) $d_{\mathcal{U}}$ -dimensional action space $\mathcal{U} \subseteq \mathbb{R}^{d_{\mathcal{U}}}$, and a dynamical model Φ (following notation from (Holt et al., 2024)). At a given time $t \in \mathcal{T} \subseteq \mathbb{R}_+$, the state of the system is denoted as $x(t) \in \mathcal{X}$, while the action of the system is $u(t) \in \mathcal{U}$. In continuous time, the evolution of the system \mathcal{S} is given by

$$\frac{dx_t}{dt} = \Phi(x(t), u(t), t) \quad (1)$$

with $\Phi : \mathcal{X} \times \mathcal{U} \times \mathcal{T} \rightarrow \mathcal{X}$.

For example, in an epidemic dynamic system, the state of the system $x(t)$ may represent the number of susceptible, infected, and recovered individuals.

Digital twins and Mechanistic Models. A digital twin of the dynamical system seeks to approximate Φ using a computational model $f_{\theta} \in \mathcal{F}$ informed by data, where $\theta \in \Theta$ denotes the parameters of the model. Here, the sets $\mathcal{F}, \Omega(\theta)$ denote the space of candidate model classes and parameter space, respectively. The parameters θ are usually calibrated manually (Kemp et al., 2021; Davids et al., 2020) or informed from data using statistical methods (Anderson, 2001; Yang et al., 2015).

In scientific domains, the system dynamics is not purely statistical but constructed grounded with domain knowledge derived from known physical, biological, or chemical processes (Marchal, 2025; Katsoulakis et al., 2024; Meyur et al., 2022; Cui et al., 2025). This structure requires each component in f to have a clear interpretation and supports reasoning about interventions and counterfactuals.

Neural-integrated Mechanistic Models. Recent work (Chopra et al., 2022; Núñez et al., 2023; Ning et al., 2023; Guan et al., 2025; Cui et al., 2025; Datta et al., 2025; Liu et al., 2022) has shown that black-box neural networks can be effective for calibrating mechanistic models. Specifically, let $f_{\beta}^{NN} : \mathcal{D} \rightarrow \Omega(\theta)$ be a neural network parameterized by β that maps the input data domain \mathcal{D} to the mechanistic model parameters space. The resulting mechanistic model is then written as f_{θ}^{mech} , where the parameter vector θ is directly provided by the f_{β}^{NN} , i.e.,

$$\theta = f_{\beta}^{NN}(D), D \in \mathcal{D}. \quad (2)$$

This yields a compositional model f in which the neural network predicts the parameters for the mechanistic component:

$$f(D) = f^{mech} \circ f_{\beta}^{NN}(D) = f^{mech}(f_{\beta}^{NN}(D)). \quad (3)$$

In this paper, we mainly consider D as a spatial-temporal

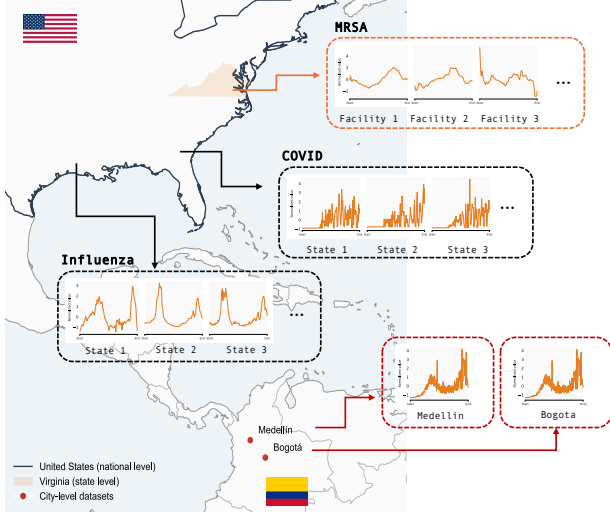


Figure 1. The datasets of the NIMM Evaluation Framework are from multiple sources and multiple levels.

dataset, where $D_{l,t}$ denotes the signals for the location $l \in \{1, \dots, L\}$ at timestamp t . The predicted parameters θ are also *spatially-* and *time-varying*, where $\theta_{l,t}$ denotes the predicted mechanistic parameter for the location l at the timestamp t . This fine-grained formulation enables the mechanistic model better adapt to heterogeneous dynamics across both space and time.

3. The NIMM Evaluation Framework.

3.1. Motivation

Despite preliminary efforts to apply LLMs to mechanistic modeling in simplified settings (Holt et al., 2024), we argue that such problem settings remain substantially detached from real-world scenarios. As a result, it remains unclear whether LLM-based systems are truly ready to generate mechanistic models for practical scientific applications.

Limitations of Prior Problem Setting. ❶ Unlike the problem setting introduced in HDTwinGen (Holt et al., 2024), where mechanistic models are used under *full observation* (i.e., all $d_{\mathcal{X}}$ -dimensional states are observable in the data), a more realistic setting is *partial observation*. In this case, the LLM must construct effective mechanistic models from partially observed real-world data, where only a subset of the $d_{\mathcal{X}}$ state variables (and in some cases, only a single dimension) is available. ❷ In many scientific applications, the goal is not merely to learn mechanistic models, but also to apply these models for diversified tasks. A desired problem setting should therefore evaluate models in diversified scenarios, rather than focusing on modeling in isolation. ❸ The problem setting in HDTwinGen further assumes that the target model f takes the form of an additive combination of a neural network and a mechanistic component, which substantially restricts the space of admissible model

structures. In contrast, our neural-integrated mechanistic formulation provides a more general modeling framework, with HDTwinGen being a special case. This generality better reflects practical modeling settings. ❹ Moreover, constructing neural-integrated mechanistic models in practice remains highly challenging, requiring substantial domain knowledge and engineering effort, and thus provides a realistic and demanding testbed for evaluating LLMs’ coding capabilities.

These considerations motivate the need for a dedicated evaluation framework that formalizes the new problem setting and systematically evaluates an LLM’s ability to perform neural-integrated mechanistic modeling.

3.2. NIMM Evaluation Framework

Datasets. Neural-integrated mechanistic modeling has been widely applied to a variety of tasks, including epidemic forecasting (Chopra et al., 2022; Guan et al., 2025; Datta et al., 2025), infection modeling (Cui et al., 2025), and alloy yield-strength prediction (Liu et al., 2022). For the **Public Health** domain, we use four popular datasets from prior work: Influenza data in the United States (Influenza-USA), methicillin-resistant Staphylococcus aureus data from Virginia (MRSA-Virginia), and COVID-19 data from two South American cities—Bogota (COVID-Bogota) and Medellin (COVID-Medellin). Figure 1 visualizes the collected datasets. Each dataset is spatiotemporal, e.g., MRSA-Virginia is a weekly dataset collected from 644 healthcare facilities in Virginia from 2016-01-03 to 2021-01-24. Figure 1 visualizes the geolocations and time series of each dataset. We also note that the signals $D_{l,t} \in \mathbb{R}^d$ might be multi-variate, containing a *subset* of $d_{\mathcal{X}}$ -dimensional states (e.g., Infection Counts) along with other contextual heterogeneous features (Point ❶). We also use datasets from other domains, including **Clinical Health** and **Materials Science**, which are described in detail in § 5.1. In this section, we present the descriptions for the **Public Health** subset.

Task Description. For public health, we adopt spatial-temporal forecasting as the main task for evaluating the effectiveness of the generated mechanistic models, which is one of the most popular tasks in epidemics (Point ❷). Formally, the problem goal is to use data till time T , namely $\{D_{:,t}\}_{t=1}^T$, to predict $\{\hat{y}_{:,t}\}_{t=T+1}^{T+H}$, e.g., the number of infections and deaths during the time period $[T+1, T+H]$, where H is the forecast horizon. More specifically, the historical data $\{D_{:,t}\}_{t=1}^T$ is used to train the compositional model f as in Equation 5. In the inference stage, given the historical data, the neural network component f^{NN} first generates spatially- and time-varying parameters $\theta_{l,t}, l \in \{1, \dots, L\}, t \in \{1, \dots, T+H\}$. Then the mechanistic component f^{mech} is run $T+H$ steps under these predicted parameters, where the last H simulation steps

serve as our forecasts.

Setups. In a typical neural-integrated mechanistic modeling pipeline, both a neural component f^{NN} and a mechanistic component f^{mech} are required (Point ③). To evaluate the LLM’s capabilities across different practical settings, we define the following scenarios: (1) **Mechanistic Mode:** completing a mechanistic model when the neural network component is already provided in the environment; (2) **Hybrid Mode:** jointly completing both the mechanistic model and the neural network model. The hybrid mode is intuitively more challenging than the mechanistic mode, as it involves a substantially larger search space.

Metrics. We aim to evaluate the *effectiveness* and *correctness* of the generated model (Point ④). For effectiveness, we employ popular metrics such as root mean square error (RMSE) for the forecasting task. Formally, the RMSE is defined as $\sqrt{\frac{1}{L \cdot H} \sum_{l,t=T+1}^{t=T+H} \|\hat{y}_{l,t} - y_{l,t}\|^2}$. Following the prior work (Chopra et al., 2022), we adopt a more practical but challenging *real-time* evaluation setup, where the training and testing period shifts over time, to avoid the cherry-picking fallacy. More details about the setup can be found in the Appendix A.4. For correctness evaluations, we use the bug count as the metric. If the generated code produces a runtime error, it is counted as buggy. To assess the NIMMGen’s capability for self-diagnosis and error correction, we report Bug Counts@20, which measures the number of buggy codes in the *last* 20 iterations.

Baselines. The LLM-based baselines include zero-shot prompting and HDTwinGen (Holt et al., 2024). In addition, we consider purely black-box models such as Transformers (Vaswani et al., 2017) and LSTMs (Hochreiter & Schmidhuber, 1997). We also include prior neural-integrated mechanistic models for comparison, including Grad-Metapopulation (Guan et al., 2025). The baselines for the other two domains are described later.

Remark 3.1 (Dual Role of the NIMM Evaluation Framework). The NIMM benchmark not only introduced a new setting to evaluate LLMs’ ability to generate code under practical scenarios, but also serves as a probe of LLM’s potential performance in scientific domains.

3.3. Evaluation Results

Table 1 reports the results of the baseline methods on the NIMM evaluation framework. We run each method three times and report the average RMSE values together with the bug counts. The experimental setup is provided in the Appendix A.4. Our results reveal several key observations. *Observation 1.* Neural-integrated modeling remains a major challenge to the existing baseline methods.

Due to the challenging setup in our evaluation framework, all the baseline methods yield relatively high RMSE values.

Observation 2. Existing LLM-based approaches frequently generate mechanistic models that fail due to run-time errors.

For example, for both zero-shot prompting and HDTwinGen, the bug counts can reach as high as 12 out of 20 generations. Despite the inherent difficulty of generating correct code for neural-integrated mechanistic models (due to their complex structure), this stark result indicates that only a limited fraction of the iterations actually generate usable models.

Observation 3. LLMs might generate mathematically valid but semantically incorrect models.

In these baselines, the primary objective is to generate mechanistic models that fit the observed data and perform forecasting through simulation. However, optimizing solely for this objective can lead LLMs to produce mechanistic models that are mathematically valid yet semantically wrong.

These models yield no run-time errors, but the specifications can hardly be interpreted by the human evaluators. In Appendix G.1, we present qualitative examples of such generated semantically wrong models.

4. Methodology

4.1. Overview

This section proposes NIMMGen, an agentic framework with a static workflow (Yu et al., 2025), to address the three observations above. Specifically, we introduce (i) a self-evolving loop consisting of a modeling agent and a reflection agent, which progressively refines model specifications through iterative optimization, addressing the challenges in Observation 1; (ii) an error-handling module that augments the agent’s memory with historical error messages to reduce repeated failures, addressing Observation 2; and (iii) a verification agent that evaluates the physical and semantic consistency of generated models, addressing Observation 3. An overview of the NIMMGen is provided in Figure 2.

Given the system prompt C , the NIMMgen performs $G \in \mathbb{N}^+$ iterations of optimizations, where each optimization loop follows a pre-defined workflow: for generation step at g , the modeling agent proposes a new candidate model based on the historical memory M^g (containing a population of top- k best models P^g , error messages Err^g , and the most recently generated reflection R^{g-1}) and the external information E^g . After the verification agent verifies the correctness of the generated model, the model will interact with the environment by optimizing the parameters of the neural-integrated mechanistic models. The feedback from the environment is then reflected and used to update the memory. After completing the G iterations, the model that yields the best performance is selected as the final model.

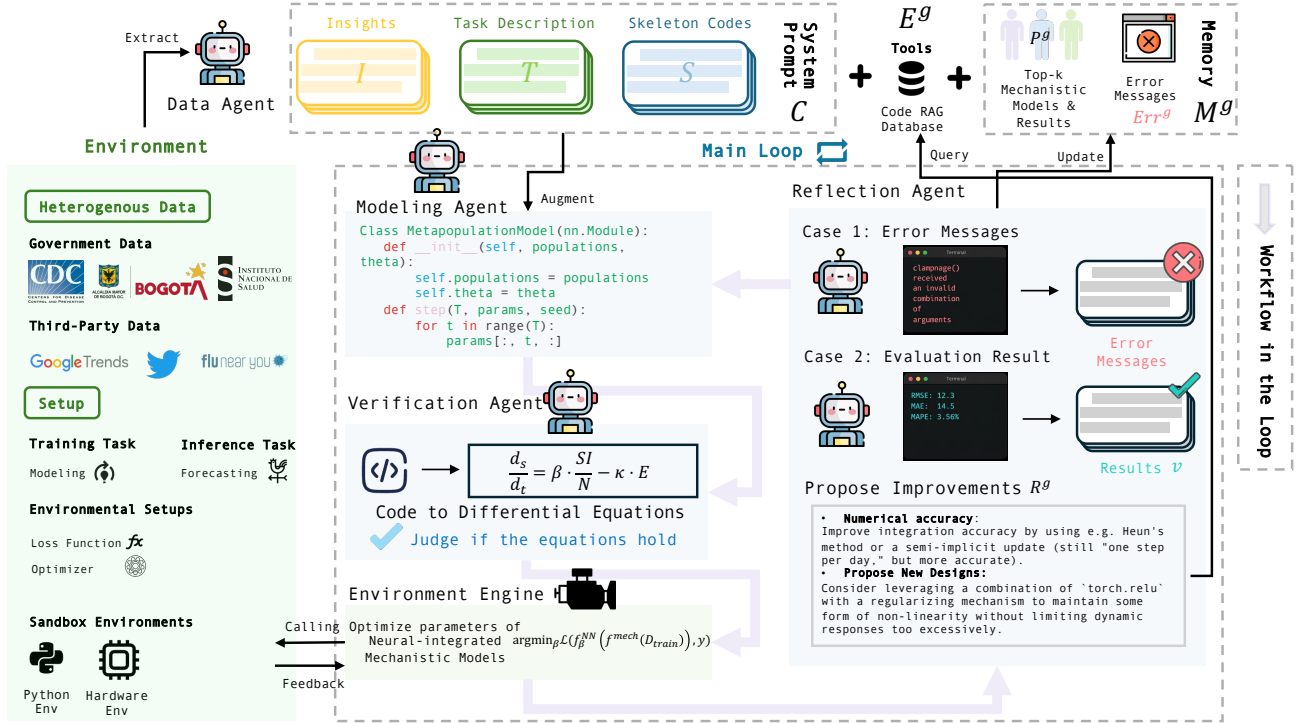


Figure 2. Overview of the proposed NIMMGen framework.

Table 1. Comparison of the effectiveness and robustness in the NIMM Evaluation Framework.

Dataset ↓	Mode	LSTM		Transformer		Grad-Metapopulation		Zero-shot		HDTwinGen		Ours	
		RMSE ↓	Bug Counts@20 ↓	RMSE ↓	Bug Counts@20 ↓	RMSE ↓	Bug Counts@20 ↓	RMSE ↓	Bug Counts@20 ^a ↓	RMSE ↓	Bug Counts@20 ↓	RMSE ↓	Bug Counts@20 ↓
COVID-Bogota	Mechanistic	633.88 _{±158.06}	/	901.96 _{±284.58}	/	1362.89 _{±165.26}	/	1102.62 _{±476.82}	4	339.13 _{±86.53}	6.27 _{±3.56}	333.91 _{±155.06}	2.67 _{±3.05}
	Hybrid							1358.24 _{±266.25}	12	765 _{±64.58}	8.67 _{±2.56}	430.42 _{±73.25}	3.33 _{±2.51}
COVID-Medellin	Mechanistic	586.88 _{±16.96}	/	552.39 _{±46.89}	/	743.25 _{±25.79}	/	908.19 _{±357.17}	4	652.72 _{±102.79}	7.65 _{±1.92}	524.3 _{±10.82}	1.67 _{±2.88}
	Hybrid							1026.25 _{±262.64}	5	675.82 _{±190.89}	3.90 _{±2.56}	562.81 _{±70.89}	2.50 _{±0.92}
Influenza-USA	Mechanistic	86.69 _{±1.73}	/	30.72 _{±0.27}	/	117.90 _{±10.93}	/	20.92 _{±5.38}	4	8.78 _{±1.49}	2.06 _{±2.25}	4.81 _{±1.50}	1.33 _{±2.31}
	Hybrid							783.49 _{±1240.58}	6	163.69 _{±40.75}	7.92 _{±1.59}	21.82 _{±8.31}	5.33 _{±4.93}
MRSA-Virginia	Mechanistic	167.08 _{±8.52}	/	127.53 _{±45.59}	/	134.05 _{±16.29}	/	516.36 _{±446.61}	6	93.23 _{±5.19}	4.76 _{±0.89}	39.83 _{±2.47}	4.33 _{±3.51}
	Hybrid							809.99 _{±392.54}	7	132.67 _{±42.82}	8.74 _{±1.26}	69.22 _{±14.62}	4.67 _{±5.50}

^a The metric is intentionally modified. We report the Bug Counts obtained by running the zero-shot method 20 times.

4.2. System Prompt and Context

System Prompt. The system prompt C is composed of three parts: (1) I : insights extracted from the data; (2) T : task description in natural languages, describing the input and output variables, and the modeling targets; (3) S : skeleton codes that describe the template of the neural-integrated mechanistic model. Here, I is obtained by employing an additional data agent to actively perceive environmental signals by enriching its context with raw data, system information, and library versions. The raw data allows the agent to directly extract insights and propose targeted designs for simulation. Including system and library version information helps the agent anticipate compatibility issues, avoid version-related errors, and understand which tools and data structures are available in advance. S is designed to provide necessary information, such as function signatures, which can guide the synthesis of executable code in a predetermined format. For illustration, we present the examples of the skeleton codes in Appendix F.

Memory Mechanism. At each generation step g , the mem-

ory contains (1) a population of top- k best models P^g across all historical runs, along with their evaluation results (2) the historical error messages Err^g from all previously failed models, and (3) the most recently generated reflection R^{g-1} in the last iteration. These provide rich contextual information for the modeling agent to reason and evolve over the successive iterations.

Code RAG Database. To further enrich the agent’s context, we introduce an external code RAG database D_{code} that allows it to proactively retrieve useful code snippets. D_{code} contains the code snippets collected from the relevant literature in the past five years. Formally, the code snippets are extracted by $E^g = h(D_{code}, R^{g-1})$, where the reflection at the last step R^{g-1} is used as the query prompt, and the code snippets $E^g \subset D_{code}$ will be returned. Detailed setups are provided in Appendix D.1.

4.3. Modeling Agent

At each generation step g , the modeling agent aims to propose novel neural-integrated mechanistic models based on

the system prompt C , memory M^g , and the external information E^g . Formally, the process can be represented as $f = f^{mech}(f_{\beta}^{NN}) \sim \text{LLM}_m(C, M^g, E^g)$. For example, in the mechanistic mode, the modeling agent constructs a set of dynamic equations that describe how different state variables evolve over time. This process involves (i) defining the compartments (i.e., state variables), (ii) specifying the flows between them using differential equations (e.g., $\frac{dE}{dt} = \frac{\eta SI}{N} - \kappa E$ in a traditional SEIRM epidemic model), and (iii) parameterizing and coupling the equations using predicted parameters from the neural component f_{β}^{NN} (e.g., η and κ in this example), thereby forming a consistent mechanistic model.

4.4. Verification Agent

To address the challenge in Observation 3, we employ a verification agent to judge and filter out the semantically wrong models. Specifically, the generated model $f^{mech}(f_{\beta}^{NN})$ is first translated into corresponding differential equations; Then the verification agent judges whether these equations are mathematically valid and consistent with established domain knowledge. By designing criteria for prompting (see Appendix F), we empirically observe that many semantically wrong mechanistic codes can be filtered out. The process can be represented as $\text{LLM}_v(f^{mech}(f_{\beta}^{NN}))$.

4.5. Environment Engine

Model Optimizations. If the model $f^{mech}(f_{\beta}^{NN})$ is verified, the agent the agent interacts with the NIMM environment using this model. Specifically, the model is trained by Equation 5 with an AdamW optimizer. Simply put, the goal is to fit the neural-integrated model to the training data till time T , namely $\{D_{:,t}\}_{t=1}^T$, to obtain the optimized β^* . The choice of the learning hyperparameters can be various, and we follow the prior works (Holt et al., 2024) with details provided in Appendix A.4.

Model Evaluations. For each model, we quantitatively evaluate its forecasting performance. The objective is to use training data up to time T , denoted by $\{D_{:,t}\}_{t=1}^T$, together with the trained model $f^{mech}(f_{\beta}^{NN})$, to predict the future trajectory $\{D_{:,t}\}_{t=T+1}^{T+H}$; that is, the number of infections and deaths over the interval $[T+1, T+H]$, where H is the forecast horizon. Importantly, the model only has access to data prior to the forecasting period. Following prior work (Chopra et al., 2022), we adopt a real-time evaluation setup (see Appendix A.4). After evaluation, the RMSE of the forecasting period (i.e., $v \leftarrow \sqrt{\frac{1}{L \cdot H} \sum_{l,t=T+1}^{t=T+H} \|\hat{y}_{l,t} - y_{l,t}\|^2}$) will be returned. Then the model will update the top- k population by $P^g \leftarrow \text{top-}k(P^{g-1} \parallel (f^{mech}(f_{\beta^*}^{NN}), v))$.

4.6. Reflection Agent

Case 1: Error-Handling. Based on the Observation 2 in the above section, we found the codes generated by SOTA LLMs are not the oracle ones - they greatly suffer from indentation errors, function calling errors, and more. We therefore design a module that enables the reflection agent to learn from past failed models and avoid repeating the same errors incurred in the past (see Appendix F for more details). Specifically, if the runtime error occurs, the agent locates the key lines of code that lead to the errors and proposes potential solutions to the errors. For the current error Err , the process is $Err^g \leftarrow Err^{g-1} \parallel Err$. We found that this simple module empirically reduces the code-level errors in the generated models (see Experiments § 5.3).

Case 2: Self-reflection. If no run-time occurs, then the agent reflects on the current top- k models P^g from multiple dimensions, including both model specification and implementation. These reflections are produced in natural language and are then added back into the context. The process can be described as $R^g \leftarrow \text{LLM}_r(P^g, v)$. Importantly, the reflection agent is not a trivial component that merely praises the modeling agent’s code. Instead, we empirically observe that it frequently proposes meaningful revisions that lead to substantial changes and measurable performance gains (see Appendix G.3).

5. Evaluation

5.1. Effectiveness Evaluations

Experimental Setup. To demonstrate the effectiveness of the NIMMGen, we evaluate its performance on three domains: (1) Public Health, (2) the Cancer dataset developed by (Holt et al., 2024) (Clinical Health), and (3) the Materials dataset from (Liu et al., 2022) (Materials Science). The Cancer benchmark is derived from a state-of-the-art biomedical pharmacokinetic–pharmacodynamic (PKPD) model of lung cancer tumor growth, which simulates the combined effects of chemotherapy and radiotherapy. Following (Holt et al., 2024), we consider three scenarios: no treatment (Lung Cancer), chemotherapy only (Lung Cancer (Chemo.)), and chemotherapy combined with radiotherapy (Lung Cancer (Chemo. & Radio.)). The Cancer dataset provides full observation of all $d_{\mathcal{X}}$ -dimensional states (rather than partial observation in the public health subset) and is used to evaluate whether LLM-generated mechanistic models can generalize to unseen trajectories, rather than to a specific forecasting task as in the public health subset. Because the Cancer dataset was not originally designed for neural-integrated pipelines, we made several manual adjustments to ensure compatibility with the NIMMGen. The specific experimental hyperparameter choices follow those in (Holt et al., 2024), which can be found in the Appendix B. The Ma-

Table 2. Comparison of NIMMGen with the baselines on the Cancer dataset.

	Zero Shot	HDTwinGen	Ours
Lung Cancer	73.25±45.1	1.69±2.05	1.41±1.58
Lung Cancer (w/ Chemo.)	53.52±16.22	1.23±0.04	0.08±0.04
Lung Cancer (w/ Chemo. & Radio.)	109.25±25.64	0.78±0.46	0.06±0.02

materials dataset follows the setup of (Liu et al., 2022), where the task is to predict alloy yield strength using a neural-integrated mechanistic model. NIMMGen is employed to optimize the mechanistic components of the model. The specific experimental setups for the Materials dataset can be found in the Appendix C.

Effectiveness on Public Health Table 1 reports the performance comparison between the NIMMGen and the baselines. Overall, the NIMMGen achieves substantially lower RMSE across all datasets. Compared with purely black-box deep learning approaches such as LSTM and Transformer, the NIMMGen not only yields better forecasting accuracy but is also inherently more interpretable to policymakers. As we show in § 5.2, the generated mechanistic models can be readily adapted to new scenarios through simple natural-language interaction and interpretable parameter modifications. Compared with the manually designed Gradmetapopulation models, the mechanistic models produced by the NIMMGen are more robust under real-time settings and exhibit stronger forecasting performance. Finally, relative to LLM-based baselines such as zero-shot prompting and HDTwinGen, the NIMMGen provides clear advantages in both forecasting accuracy and the likelihood that the generated models run successfully.

Moreover, we also observe that the hybrid mode generally shows a slightly worse performance than the mechanistic mode. Although this may appear counterintuitive, it aligns with our expectations: In the hybrid mode, the LLM is expected tune both the mechanistic part and the neural network part, which might be harder to synchronize. The challenge also comes from that fact that the searching space of the hybrid space is considerably larger compared to the mechanistic mode. Therefore, given the same budget, the hybrid mode shows a slightly worse performance.

Effectiveness on Clinical Health. Table 2 compares the three LLM-based approaches on the cancer dataset. As shown, our pipeline consistently achieves lower RMSE errors than the two baselines, by over 16.56% in the Lung Cancer dataset, and 92.31% in the Lung Cancer (w/ Chemo. & Radio) dataset in average, demonstrating the advantages brought by the neural-integrated design.

Effectiveness on Materials Science. As shown in Table 5, the resulting neural-integrated model achieves significantly better performance than the purely neural network baseline.

These experimental results demonstrate the comprehensive

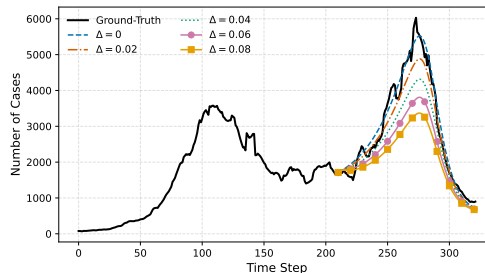


Figure 3. Observed and simulated epidemic trajectories under simulated social distancing policies.

ability in handling the three domains across different scientific domains, further suggesting its broad potential in building effective mechanistic models.

5.2. Counterfactual Intervention Simulations

In this section, we show the potential validity of the models generated by NIMMGen with a counterfactual intervention.

Counterfactual intervention simulation is a widely used application of mechanistic models, aiming to quantify how hypothetical policies (e.g., social distancing) alter epidemic trajectories relative to the observed baseline (Ge et al., 2021; Rădulescu et al., 2020; Ventura et al., 2022). In particular, social distancing policies primarily affect disease transmission by reducing effective contact rates. We therefore simulate social distancing by adjusting the transmission-related component of the model after a given time T' . Let $\theta_{l,t,\bar{\gamma}}$ denote the effective transmission rates $\bar{\gamma}$ produced by the neural component f_{β}^{NN} at time t for location l . We define

$$\theta_{l,t,\bar{\gamma}} = \begin{cases} \theta_{l,t,\bar{\gamma}}, & t < T' \\ (1 - \Delta) \cdot \theta_{l,t,\bar{\gamma}}, & t \geq T', \forall 1 < l \leq L \end{cases} \quad (4)$$

where Δ denotes the strength of social distancing intervention and Δ a larger Δ corresponds to stronger reductions in population contact.

Figure 3 shows the intervention experiments on the COVID-Bogota dataset ($L = 1$) with $T' = 270$. The neural-integrated mechanistic model is chosen as the best one generated by the NIMMGen. As expected, increasing the strength of the simulated social distancing intervention results in systematic reductions in epidemic peak magnitude and cumulative case counts. Notably, this experiment does not aim to assess the real-world effectiveness of specific policies, as counterfactual ground truth is inherently unavailable. Instead, the objective is to evaluate whether the generated mechanistic models respond to intervention parameters in a manner consistent with epidemiological principles.

5.3. Further Analysis

What has been changed during the Optimization? Fig-

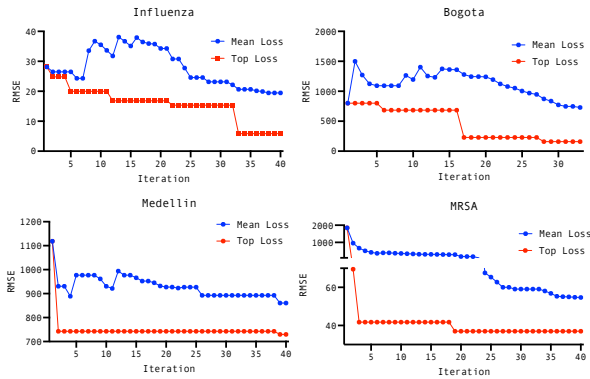


Figure 4. Loss curve along with the iterations.

Table 3. Performance Comparison under Different LLM Models.

Model Type	Model Name	Influenza-USA	MRSA-Virginia
Proprietary LLM	GPT-4.1	4.81±1.50	39.83±2.47
	GPT-4o	8.17±2.54	44.36±7.94
	GPT-5-mini	38.41±20.37	82.41±26.57
Open-source LLM	Qwen2.5-32B-Coder	25.35±3.67	96.75±42.67
	Qwen3-30B-Coder	19.15±8.76	81.52±34.53

Figure 4 visualizes the loss curve over the course of optimization. We plot both the average RMSE validation loss of all historically generated mechanistic models and the best (lowest) RMSE validation loss achieved so far. As shown, the mean loss exhibits a decreasing trend, suggesting that models generated at later iterations progressively improve the population through guided optimization rather than purely stochastic trial-and-error. The best loss also steadily decreases with iterations, demonstrating that the NIMMGen can continuously refine the model during the search process. To further understand what changes in the mechanistic code contribute to these improvements, we qualitatively analyze the mechanistic programs throughout optimization and summarize the key modifications in Table 9.

Sensitivity of the Hyper-parameters. In Table 3, we compare the performance of the NIMMGen with different base LLMs, including proprietary models such as GPT-4.1, GPT-5, and GPT-5.2, and two frontier open-source coding models, including Qwen2.5-32B-Coder and Qwen3-30B-Coder. The detailed setups are provided in Appendix D.2. In Table 6, we compare the performance of the NIMMGen under different iteration numbers, ranging from 10 to 80.

Ablation Studies. Table 7 compares the average bug counts in the first and last 20 iterations, before and after applying the error-correction module. The experiments are conducted on the Influenza-USA dataset, with hyperparameters set to default values. As shown, the error-correction module significantly reduces the number of bugs, especially in the last 20 iterations, suggesting that our agentic framework enables the model to adaptively learn how to debug and avoid errors during the optimization process. Table 8 also

compares the performance with and without the verification agent. The analysis are detailed in Appendix E.1.

6. Related Works

LLMs for Mechanistic Modeling. Large language models (LLMs) have been extensively used for scientific coding tasks (Tang et al., 2024; White et al., 2023; Zhang et al., 2025; Kwok et al., 2024). However, most existing approaches focus on one-shot code generation, rather than iterative optimization of model structures. AlphaEvolv (Novikov et al., 2025) proposed an evolutionary coding framework that automatically generates, evaluates, and refines computer programs for scientific and algorithmic discovery. Nevertheless, it is designed as a general-purpose system, whereas our work focuses specifically on mechanistic modeling, a subfield of scientific coding that places stronger emphasis on validity and knowledge grounding.

The most closely related work to ours is HDTwinGen (Holt et al., 2024). However, as discussed in the previous sections, their experimental setup substantially oversimplifies real-world scenarios, and their modeling assumption—namely, a simple additive combination of neural and mechanistic components—is often impractical in realistic applications.

Sequential Deep Neural Networks. Sequential Deep Neural Networks (DNNs) can be adapted to the mechanistic modeling task. Specifically, rather than directly learning a single function f^{mech} , the sequential DNNs aim to learn a black-box function f that aims to directly predict the system state at the next time step based on a window of historical states. Typical architectures such as RNNs (Elman, 1990), LSTMs (Hochreiter & Schmidhuber, 1997), and Transformers (Vaswani et al., 2017) have been widely applied in this setting. Although sequential DNNs show promising performance in capturing complex dynamics in the data, they are heavily relying on training data for generalization and lack substantive interpretability.

7. Conclusion

We first propose NIMM, an evaluation framework with the novel neural-integrated mechanistic modeling problem setting. Based on the evaluation results on the baselines, we identify some key challenges in the current baseline methods. Motivated by these findings, we design an improved agentic framework, NIMMGen, that explicitly improves code correctness and practical validity during iterative refinement. Experiments across three domains demonstrate the effectiveness of the NIMMGen. Despite the promising performance, several questions are still interesting: (1) Can we design a more reliable and efficient method for model verification apart from using LLMs? and (2) Would information from other modalities be useful for generating more

effective mechanistic models?

Impact Statement

This paper proposed an evaluation framework for evaluating the LLM’s capability in generating neural-integrated mechanistic models, and an agentic framework for enabling the LLMs to optimize the neural-integrated mechanistic models. Our main aim is to explore potentially effective methods for generating the neural-integrated mechanistic models.

References

- Adhikari, B., Xu, X., Ramakrishnan, N., and Prakash, B. A. Epideep: Exploiting embeddings for epidemic forecasting. In *Proceedings of the 25th ACM SIGKDD international conference on knowledge discovery & data mining*, pp. 577–586, 2019.
- Adiga, A., Kuhlman, C. J., Marathe, M. V., Mortveit, H. S., Ravi, S. S., and Vullikanti, A. Graphical dynamical systems and their applications to bio-social systems. In *International Journal of Advances in Engineering Sciences and Applied Mathematics*, pp. 1–19. Springer, 2018. Online version appeared in Dec. 2018.
- Anderson, J. L. An ensemble adjustment kalman filter for data assimilation. *Monthly weather review*, 129(12):2884–2903, 2001.
- Borg, C. K., Frey, C., Moh, J., Pollock, T. M., Gorsse, S., Miracle, D. B., Senkov, O. N., Meredig, B., and Saal, J. E. Expanded dataset of mechanical properties and observed phases of multi-principal element alloys. *Scientific Data*, 7(1):430, 2020.
- Chopra, A., Rodríguez, A., Subramanian, J., Quera-Bofarull, A., Krishnamurthy, B., Prakash, B. A., and Raskar, R. Differentiable agent-based epidemiology. *arXiv preprint arXiv:2207.09714*, 2022.
- Cramer, E. Y., Ray, E. L., Lopez, V. K., Bracher, J., Brennen, A., Castro Rivadeneira, A. J., Gerding, A., Gneiting, T., House, K. H., Huang, Y., et al. Evaluation of individual and ensemble probabilistic forecasts of covid-19 mortality in the united states. *Proceedings of the National Academy of Sciences*, 119(15):e2113561119, 2022.
- Cui, J., Heavey, J., Klein, E., Madden, G. R., Sifri, C. D., Vullikanti, A., and Prakash, B. A. Identifying and forecasting importation and asymptomatic spreaders of multi-drug resistant organisms in hospital settings. *NPJ Digital Medicine*, 8(1):147, 2025.
- Datta, R., Cui, J., Madden, G. R., and Vullikanti, A. Calypso: Forecasting and analyzing mrsa infection patterns with community and healthcare transmission dynamics. *arXiv preprint arXiv:2508.13548*, 2025.
- Davids, A., Rand, G. d., Georg, C.-P., Koziol, T., and Schasfoort, J. Sabcom: A spatial agent-based covid-19 model. *MedRxiv*, pp. 2020–07, 2020.
- Elman, J. L. Finding structure in time. *Cognitive science*, 14(2):179–211, 1990.
- Ge, Y., Chen, Z., Handel, A., Martinez, L., Xiao, Q., Li, C., Chen, E., Pan, J., Li, Y., Ling, F., et al. The impact of social distancing, contact tracing, and case isolation interventions to suppress the covid-19 epidemic: A modeling study. *Epidemics*, 36:100483, 2021.
- Guan, Z., Zhao, Z., Tian, F., Nguyen, D., Bhattacharjee, P., Tandon, R., Prakash, B. A., and Vullikanti, A. A framework for multi-source privacy preserving epidemic analysis. *arXiv preprint arXiv:2506.22342*, 2025.
- Hochreiter, S. and Schmidhuber, J. Long short-term memory. *Neural computation*, 9(8):1735–1780, 1997.
- Holt, S., Liu, T., and van der Schaar, M. Automatically learning hybrid digital twins of dynamical systems. *Advances in Neural Information Processing Systems*, 37:72170–72218, 2024.
- Kamarthi, H., Rodríguez, A., and Prakash, B. A. Back2future: Leveraging backfill dynamics for improving real-time predictions in future. *arXiv preprint arXiv:2106.04420*, 2021.
- Kamarthi, H., Kong, L., Rodríguez, A., Zhang, C., and Prakash, B. A. Camul: calibrated and accurate multi-view time-series forecasting. In *Proceedings of the ACM Web Conference 2022*, pp. 3174–3185, 2022.
- Karniadakis, G. E., Kevrekidis, I. G., Lu, L., Perdikaris, P., Wang, S., and Yang, L. Physics-informed machine learning. *Nature Reviews Physics*, 3(6):422–440, 2021.
- Karpatne, A., Kannan, R., and Kumar, V. *Knowledge guided machine learning: Accelerating discovery using scientific knowledge and data*. CRC Press, 2022.
- Katsoulakis, E., Wang, Q., Wu, H., Shahriyari, L., Fletcher, R., Liu, J., Achenie, L., Liu, H., Jackson, P., Xiao, Y., et al. Digital twins for health: a scoping review. *NPJ digital medicine*, 7(1):77, 2024.
- Kemp, F., Proverbio, D., Aalto, A., Mombaerts, L., d’Hérouël, A. F., Husch, A., Ley, C., Gonçalves, J., Skupin, A., and Magni, S. Modelling covid-19 dynamics and potential for herd immunity by vaccination in austria, luxembourg and sweden. *Journal of Theoretical Biology*, 530:110874, 2021.

- Kwok, K. O., Huynh, T., Wei, W. I., Wong, S. Y., Riley, S., and Tang, A. Utilizing large language models in infectious disease transmission modelling for public health preparedness. *Computational and Structural Biotechnology Journal*, 23:3254–3257, 2024.
- Kwon, W., Li, Z., Zhuang, S., Sheng, Y., Zheng, L., Yu, C. H., Gonzalez, J., Zhang, H., and Stoica, I. Efficient memory management for large language model serving with pagedattention. In *Proceedings of the 29th symposium on operating systems principles*, pp. 611–626, 2023.
- Liu, S., Lee, K., and Balachandran, P. V. Integrating machine learning with mechanistic models for predicting the yield strength of high entropy alloys. *Journal of Applied Physics*, 132(10):105105, 2022.
- Marathe, M. and Vullikanti, A. Computational epidemiology. *Communications of the ACM*, 56(7):88–96, 2013.
- Marchal, I. Applications of digital twins in medicine. *nature biotechnology*, 43(10):1606–1612, 2025.
- Maresca, F. and Curtin, W. A. Mechanistic origin of high strength in refractory bcc high entropy alloys up to 1900k. *Acta Materialia*, 182:235–249, 2020.
- Meyur, R., Vullikanti, A., Swarup, S., Mortveit, H. S., Centeno, V., Phadke, A., Poor, H. V., and Marathe, M. V. Ensembles of realistic power distribution networks. *Proceedings of the National Academy of Sciences*, 119(42):e2205772119, 2022.
- National Academies of Sciences, Engineering, and Medicine. Foundational research gaps and future directions for digital twins. 2023.
- Niederer, S. A., Sacks, M. S., Girolami, M., and Willcox, K. Scaling digital twins from the artisanal to the industrial. *Nature Computational Science*, 1(5):313–320, 2021.
- Ning, X., Jia, L., Wei, Y., Li, X.-A., and Chen, F. Epi-dnns: Epidemiological priors informed deep neural networks for modeling covid-19 dynamics. *Computers in biology and medicine*, 158:106693, 2023.
- Novikov, A., Vū, N., Eisenberger, M., Dupont, E., Huang, P.-S., Wagner, A. Z., Shirobokov, S., Kozlovskii, B., Ruiz, F. J., Mehrabian, A., et al. Alphaevolve: A coding agent for scientific and algorithmic discovery. *arXiv preprint arXiv:2506.13131*, 2025.
- Núñez, M., Barreiro, N. L., Barrio, R. A., and Rackauckas, C. Forecasting virus outbreaks with social media data via neural ordinary differential equations. *Scientific Reports*, 13(1):10870, 2023.
- Rădulescu, A., Williams, C., and Cavanagh, K. Management strategies in a seir-type model of covid 19 community spread. *Scientific reports*, 10(1):21256, 2020.
- Shaman, J., Karspeck, A., Yang, W., Tamerius, J., and Lipsitch, M. Real-time influenza forecasts during the 2012–2013 season. *Nature communications*, 4(1):2837, 2013.
- Tang, X., Qian, B., Gao, R., Chen, J., Chen, X., and Gerstein, M. B. Biocoder: a benchmark for bioinformatics code generation with large language models. *Bioinformatics*, 40(Supplement_1):i266–i276, 2024.
- Thorve, S., Baek, Y. Y., Swarup, S., Mortveit, H., Marathe, A., Vullikanti, A., and Marathe, M. High resolution synthetic residential energy use profiles for the united states. *Scientific Data*, 10(1):76, 2023.
- Vaswani, A., Shazeer, N., Parmar, N., Uszkoreit, J., Jones, L., Gomez, A. N., Kaiser, Ł., and Polosukhin, I. Attention is all you need. *Advances in neural information processing systems*, 30, 2017.
- Venkatramanan, S., Chen, J., Fadikar, A., Gupta, S., Higdon, D., Lewis, B., Marathe, M., Mortveit, H., and Vullikanti, A. Optimizing spatial allocation of seasonal influenza vaccine under temporal constraints. *PLoS computational biology*, 15(9):e1007111, 2019.
- Ventura, P. C., Aleta, A., Rodrigues, F. A., and Moreno, Y. Modeling the effects of social distancing on the large-scale spreading of diseases. *Epidemics*, 38:100544, 2022.
- Ward, L., Agrawal, A., Choudhary, A., and Wolverton, C. A general-purpose machine learning framework for predicting properties of inorganic materials. *npj Computational Materials*, 2(1):16028, 2016.
- White, A. D., Hocky, G. M., Gandhi, H. A., Ansari, M., Cox, S., Wellawatte, G. P., Sasmal, S., Yang, Z., Liu, K., Singh, Y., et al. Assessment of chemistry knowledge in large language models that generate code. *Digital Discovery*, 2(2):368–376, 2023.
- Yang, W., Lipsitch, M., and Shaman, J. Inference of seasonal and pandemic influenza transmission dynamics. *Proceedings of the National Academy of Sciences*, 112(9):2723–2728, 2015.
- Yin, B. and Curtin, W. A. First-principles-based prediction of yield strength in the rhiprdptnicu high-entropy alloy. *npj Computational Materials*, 5(1):14, 2019.
- Yu, C., Cheng, Z., Cui, H., Gao, Y., Luo, Z., Wang, Y., Zheng, H., and Zhao, Y. A survey on agent workflow-status and future. In *2025 8th International Conference on Artificial Intelligence and Big Data (ICAIBD)*, pp. 770–781. IEEE, 2025.

Zhang, Y., Han, Y., Chen, S., Yu, R., Zhao, X., Liu, X., Zeng, K., Yu, M., Tian, J., Zhu, F., et al. Large language models to accelerate organic chemistry synthesis. *Nature Machine Intelligence*, pp. 1–13, 2025.

A. NIMM Evaluation Framework (Public Health)

A.1. Overview

The NIMM evaluation framework consists of four epidemiological datasets (Cui et al., 2025; Guan et al., 2025; Chopra et al., 2022; Datta et al., 2025) spanning multiple diseases, spatial resolutions, and temporal granularities. It is designed to reflect realistic challenges encountered in public health surveillance, including spatial heterogeneity and varying observation frequencies. Table 4 summarizes the datasets used to construct the NIMM evaluation framework, and Figure 1 visualizes the geolocations and aggregated time series for each dataset.

A.2. Dataset

The evaluation framework covers three infectious diseases, i.e., COVID, Influenza, and Methicillin-resistant *Staphylococcus aureus* (MRSA), and includes data from both macro-level surveillance systems and facility-level administrative records. The shape of each dataset can be described using three dimensions: (# Locations, # Timestamps, # Features).

COVID-Bogota & COVID-Medellin These are City-level COVID-19 datasets collected from the Colombia NIH². The dataset contains daily observations of 343 days. Following (Guan et al., 2025), we adopt 11 features collected from heterogenous sources, including:

- **Mobility signals.** These signals originate from records of visits to points of interest (POIs) across different regions. According to Google Mobility³, daily changes in visits to various POI categories are collected and reported relative to the baseline period from January 3 to February 6, 2020. We extract six time-series features capturing mobility changes under different scenarios, including `retail_and_recreation` and `grocery_and_pharmacy`.
- **Google Trends signals.** Google provides search trend statistics for user-specified keywords⁴. We collect search

²<https://www.ins.gov.co/Noticias/Paginas/coronavirus-casos.aspx>

³https://www.gstatic.com/covid19/mobility/Global_Mobility_Report.csv

⁴<https://trends.google.com/trends/explore?date=today>

trends for four COVID-19–related keywords, such as “covid-19 en Colombia,” “covid-19 hoy,” and “covid-19 Bogotá,” resulting in three time-series features.

- **Infection-related context.** The Colombian National Institute of Health (NIH) reports daily COVID-19 infection and mortality counts, serving as the official data source in Colombia. From this source, we derive two time-series features.

COVID-Bogota and COVID-Medellin are both collected on the city-level. Therefore, the final shape of the two datasets is (1, 343, 11).

Influenza-USA State-level influenza datasets. Following (Chopra et al., 2022), we adopt 14 signals.

- **Symptoms.** This contains 13 different time series symptoms features collected from the Google symptoms dataset⁵, including Fever, Cough, and Sore throat.
- **influenza-like-illness (ILI).** This is collected by the CDC and records the influenza-like-illness across different timestamps.

Influenza-USA is collected from 51 states in the USA. Therefore, the final shape of the Influenza-USA dataset is (51, 191, 14).

MRSA-Virginia Facility-level MRSA datasets are collected from the Virginia All Payers Insurance Claims dataset (APCD). Built on top of (Datta et al., 2025), we adopt four signals:

- **Demographical signals.** This includes number of MRSA cases for each age groups. (We have 15 ages groups and therefore we have 15 features)
- **Prescriptions.** Number of Prescription claims listed in the insurance data along with the timestamps.
- **MRSA Infections.** The number of infection counts corresponding to the MRSA.

MRSA-Virginia is collected from 644 healthcare facilities in the Virginia state. Therefore, the final shape of the MRSA-Virginia dataset is (644, 244, 20).

A.3. Code Generation Modes

We consider two types of code generations modes: *mechanistic model* and *hybrid mode*. In the mechanistic mode,

⁵<https://github.com/GoogleCloudPlatform/covid-19-open-data/blob/main/docs/table-search-trends.md>

Table 4. Statistical Description of the datasets used in the NIMM Evaluation Framework (Public Health).

Dataset Name	Data Source	Observation Period	Spatial Granularity	# Locations	Temporal Granularity	# Timestamps	Disease	# Features	Target
COVID-Bogota	Colombia NIH	2020-04-12 - 2021-01-30	City-level	1	Daily	343 (d)	COVID	11	Infection Counts
COVID-Medellin	Colombia NIH	2020-04-12 - 2021-01-30	City-level	1	Daily	343 (d)	COVID	11	Infection Counts
Influenza-USA	CDC	2017-W34 - 2021-W15 ¹	State-level	51	Weekly	191 (w)	Influenza	15	Infection Counts
MRSA-Virginia	Virginia APCD	2016-W01 - 2021-W04	Facility-level	644	Weekly	244 (w)	MRSA	20	Infection Counts

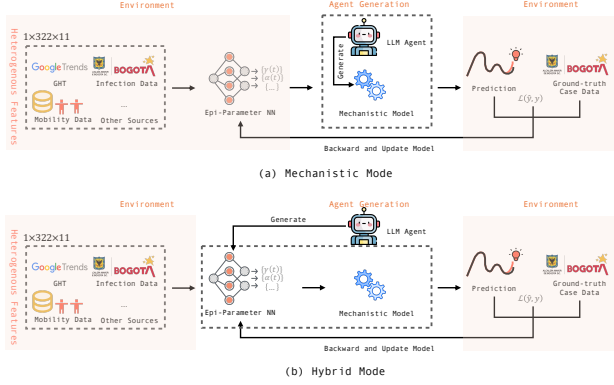


Figure 5. Experimental setup. (a) Mechanistic mode. (b) Hybrid Mode.

the agent is responsible for generating the codes for f^{mech} only, while the f^{neural} is predefined in the environment. In particular, in the mechanistic mode, we use the CalibNN designed by (Chopra et al., 2022), which has been demonstrated to be effective in extracting the information from heterogeneous data sources across multiple datasets. In the full model mode, the agent is responsible for generating the full model $f^{mech}(f^{NN}(\cdot))$.

A.4. Task & Evaluation

Task Description In the NIMM evaluation framework, we mainly focus on forecasting, which is one of the most popular tasks in epidemics. Formally, the goal in the forecasting problem is to use data till time T , namely $\{\mathbf{x}_t\}_{t=1}^T$, and predict $\{\mathbf{x}_t\}_{T+1}^{T+H}$ i.e., the number of infections and deaths during the time period $[T + 1, T + H]$, where H is the forecast horizon.

Training and Inference During training, we aim to calibrate the composite model $f(\cdot) = f^{mech}(f_{\beta}^{NN}(\cdot))$ from the training data $\{D_{:,t}\}_{t=1}^T$. Specifically, the neural network $\theta = f_{\beta}^{NN}(\{D_{:,t}\}_{t=1}^T)$ takes the entire training sequence as input and predicts the parameters of the mechanistic model. These predicted parameters θ are then used to instantiate the mechanistic model f^{mech} , which is executed for T time steps to generate simulations for the target state (e.g., infection counts), i.e., $\{\hat{y}_{:,t}\}_{t=1}^T$. The training objective is to minimize the root mean squared error (RMSE) between the simulated target values $\{\hat{y}_{:,t}\}_{t=1}^T$ and the ground-truth target

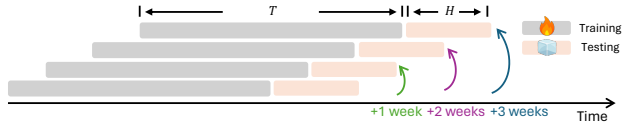


Figure 6. Real-time evaluation Setup.

observations $\{y_{:,t}\}_{t=1}^T$:

$$\beta^* = \arg \min_{\beta} \text{RMSE}(\{\hat{y}_{:,t}\}_{t=1}^T, \{y_{:,t}\}_{t=1}^T), \quad (5)$$

where $\{\hat{y}_{:,t}\}_{t=1}^T = f^{mech}(f_{\beta}^{NN}(\{D_{:,t}\}_{t=1}^T))$.

At inference time, we perform forecasting by running the calibrated composite model for $T + H$ steps. The first T steps reproduce the observed period, while the additional H steps generate predictions for the future horizon $[T + 1, \dots, T + H]$.

Real-time Evaluation Following the popular real-time evaluation pipelines in the epidemics (Chopra et al., 2022; Adhikari et al., 2019; Kamarthi et al., 2022; Shaman et al., 2013), we mainly evaluate the performance of the constructed models using the *real-time forecasting* setup. We simulate real-time forecasting by forcing the models to train only using data available until each of the prediction dates and make predictions for 4 weeks ahead in the future. Data revisions in public health data are large and may affect evaluation and conclusions (Cramer et al., 2022; Kamarthi et al., 2021), therefore, we utilize fully revised data following previous papers on methodological advances.

Specifically, we shift the training time window to 1, 2, and 3 weeks ahead to simulate the real-time setting. Figure 6 visualizes the real-time evaluation setups.

Environment Setup The learning rate of the training is set as $5e^{-4}$ with AdamW as the optimizer. The training iteration is set to 1000 to ensure convergence. The H is set to be 8 (weeks) for Influenza-USA and MRSA-Virginia datasets, and 28 (days) for the COVID-Bogota and COVID-Medellin datasets. The T is chosen depending on different datasets. For the COVID-Bogota and COVID-Medellin, the default T is 294 days (42 weeks); For the Influenza-USA, the default T is 191 (weeks); For the MRSA-Virginia, the default T is 244 (weeks).

To use the COVID-Bogota and COVID-Bogota dataset for real-time evaluation, the training period will shift from

[1, ..., 294] to [21, ..., 315], and the testing period will accordingly shift from [295, ..., 322] to [316, ..., 343].

To use the Influenza-USA dataset for real-time evaluation, the training period will shift from [1, ..., 179] to [4, ..., 182], and the testing period will accordingly shift from [180, ..., 188] to [183, ..., 191].

To use the MRSA-Virginia dataset for real-time evaluation, the training period will shift from [1, ..., 232] to [4, ..., 235], and the testing period will accordingly shift from [233, ..., 241] to [236, ..., 244].

Experimental Setup The default iteration number for the NIMMGen pipeline is set to 40. All experiments are conducted on two A100 GPUs. We use GPT-4.1 as the default backbone LLM.

A.5. Baselines

As stated in the main text, we opt to use the following three types of baselines.

A.5.1. NEURAL SEQUENCE MODELS

LSTM Model We adopt a simple LSTM model consisting of one LSTM layer with hidden size 32, followed by a dense layer with hidden size 16, a rectified linear unit (ReLU) activation function, and a dropout layer with a dropout rate of 0.2. The output layer is a dense layer with linear activation and L_2 kernel regularization with a penalty factor of 0.01. The input dataset $\{D_t\}_{t=1}^T$ is first segmented into overlapping five-timestamp windows, where the first four timestamps (D_{t-4}, \dots, D_{t-1}) are used as input features and the last timestamp D_t is used as the prediction target. Formally, the model learns a mapping

$$\hat{D}_t = f^{\text{LSTM}}(D_{t-4}, D_{t-3}, D_{t-2}, D_{t-1}).$$

In the inference stage, we generate H -step-ahead forecasts in an auto-regressive manner. Starting from the last observed window ($D_{T-3}, D_{T-2}, D_{T-1}, D_T$), the model predicts

$$\hat{D}_{T+1} = f^{\text{LSTM}}(D_{T-3}, D_{T-2}, D_{T-1}, D_T).$$

This prediction is then fed back into the input window to generate subsequent forecasts:

$$\hat{D}_{T+h} = f^{\text{LSTM}}(\hat{D}_{T+h-4}, \hat{D}_{T+h-3}, \hat{D}_{T+h-2}, \hat{D}_{T+h-1}),$$

$$h = 2, \dots, H, \quad (6)$$

where observed values are used when available and predicted values are used once the forecasting horizon extends beyond the training data. This iterative process yields the final H -step forecast $\{\hat{D}_{T+1}, \dots, \hat{D}_{T+H}\}$.

Transformer Model We first encode input dimension of the observations into an embedding vector dimension of size 64 through a linear network, followed by the addition of a standard positional encoder. Then, this is fed into the Transformer encoder layers, which had a head size of 4 and contains three layers of Transformer blocks. The final output is mapped back to the input dimension by using an additional linear layer. The training and the inference strategies are similar to those in the LSTM model.

A.5.2. EXISTING NEURAL-INTEGRATED MECHANISTIC MODELS

Grad Meta-population Model A meta-population model requires two key inputs: a contact matrix $\mathcal{C} \in \mathbb{R}^{m \times m}$ and a population vector $N \in \mathbb{R}^m$, where $m = |\mathcal{G}|$ is the number of groups. Each entry $C_{i,j} \in \mathcal{C}$ represents the contact probability between the populations in groups i and j , while each entry $N^j \in N$ records the population of group j . Following (Venkatramanan et al., 2019), the effective number of infected individuals and the effective population of group j after daily movement are defined as:

$$I_j^{\text{EFF}} = \sum_i C_{i,j} I_i, \quad N_j^{\text{EFF}} = \sum_i C_{i,j} N_i \quad (7)$$

where "EFF" (effective) refers to infections accounted including infected individuals between different subpopulations due to transmissibility and mobility. The conditional force of infection for group j is then given by:

$$\beta_j^{\text{EFF}} = \beta \frac{I_j^{\text{EFF}}}{N_j^{\text{EFF}}}. \quad (8)$$

For each group $i \in [1, \dots, m]$, the epidemic evolution $\mathcal{Z}_i = [S_i, E_i, I_i, R_i, M_i]$ from day t to day $t+1$ is formulated as:

$$\mathcal{Z}_i(t+1) = \mathcal{Z}_i(t) + \Delta \mathcal{Z}_i(t), \quad \text{where}$$

$$\Delta S_i(t) = - \sum_{j=1}^m C_{i,j} \beta_j^{\text{EFF}} S_i(t) + \delta(t) R_i(t),$$

$$\Delta E_i(t) = \sum_{j=1}^m C_{i,j} \beta_j^{\text{EFF}} S_i(t) - \alpha(t) E_i, \quad (9)$$

$$\Delta I_i(t) = \alpha(t) E_i(t) - (\gamma(t) + \eta(t)) I_i(t),$$

$$\Delta R_i(t) = \gamma(t) I_i(t) + (1 - \delta(t)) R_i(t),$$

$$\Delta M_i(t) = \eta(t) I_i(t).$$

where our forecasting objective $\Delta I_i(t)$ represents the number of newly infected individuals in age group i at time t . Running the meta-population model for T time steps, it outputs the aggregated new cases over all the age groups for the entire training period:

$$\hat{y}_t := \sum_{i=1}^m \Delta I_i(t), \quad \forall 1 \leq t \leq T. \quad (10)$$

Following (Guan et al., 2025), we calibrate the model with a CalibNN. We follow the same implementations as outlined in GitHub⁶.

A.5.3. LLM-BASED GENERATIONS

Zero-shot For zero-shot generation, we prompt the LLM model with the exact task description and the skeleton codes as our pipeline. However, it only generates the code once and incorporates no criticism from the reflection agent.

HDTwinGen (Holt et al., 2024) We adopt the same implementation as described in the official GitHub⁷.

B. NIMM (Clinical Health) Setup

In the original HDTwinGen setup of the Cancer dataset, the mechanistic model is designed to learn a transition from the current state $x_t \in \mathbb{R}^{d_x}$ to the next state x_{t+1} . To adapt this dataset to our neural-integrated framework, we introduce a neural network f^{NN} that takes the current state x_t as input and outputs the parameters of the cancer mechanistic model. The mechanistic model then uses these parameters, together with the current state x_t , to produce the state at the next time step.

C. NIMM (Materials Science) Setup

The considered task is to predict the temperature-dependent yield strength of single-phase Face-Centered Cubic (FCC) / Body-Centered Cubic (BCC) high-entropy alloys (HEAs) by integrating a neural network with a physics-based mechanistic model (Yin & Curtin, 2019; Maresca & Curtin, 2020). Similar to the setup in NIMM, the neural network component is used to predict key mechanistic parameters from alloy composition data D . Then these predicted parameters are used to propagate through a mechanistic model, yielding the final yield strength prediction. For FCC alloys, the dataset D contains 29 HEAs and room temperature yield strength, where each input feature characterizes composition-based descriptors derived from elemental properties (Ward et al., 2016; Liu et al., 2022) (e.g., valence electrons, atomic volume). For BCC alloys, the dataset D contains 130 HEAs with temperature-dependent yield strength data, where each input feature also characterizes composition-based descriptors derived from elemental properties (Borg et al., 2020) (e.g., valence electrons, atomic volume).

⁶<https://github.com/GuanZihan/GradMetapopulation.git>

⁷<https://github.com/samholt/HDTwinGen>

D. Detailed Setups

D.1. RAG Tool

We construct the RAG database using Qwen/Qwen3-Embedding-0.6B as the embedding model. During the inference stage of the RAG module, the top-3 most similar code chunks are retrieved and appended to the task prompt as contextual augmentation. The code repository is built by collecting epidemic models proposed in papers published over the past five years and incorporating their released implementations, when available, to construct the RAG database.

D.2. Open-source Models Setup

To improve the reproducibility of the NIMMGen, we set the temperature to 0 for all experiments using open-source models. The `max_tokens` parameter is set to 2048. We use vLLM (Kwon et al., 2023) to deploy the open-source models and adopt the OpenAI API schema to communicate with them. All experiments are conducted on two A100 GPUs. The two open-source models are Qwen/Qwen3-Coder-30B-A3B-Instruct⁸ and Qwen/Qwen2.5-Coder-32B-Instruct⁹ respectively.

Table 5. RMSE comparison between the NIMMGen and the pure black-box neural networks on the yield strength prediction task.

	Neural Network	Ours
FCC	213.13 \pm 58.51	139.19 \pm 29.25
BCC	235.10 \pm 15.55	180.13 \pm 68.99

E. More Results

Table 6. Performance Comparison under Different Iterations.

	10	20	40	80
Influenza-USA	18.92 \pm 2.76	14.26 \pm 2.79	4.81 \pm 1.50	4.40 \pm 0.95

E.1. More Results on the Ablation Studies

Table 8 reports the performance with and without the Verification Agent on the Influenza-USA dataset. The results indicate that the Verification Agent alone does not exert a monotonic effect on the final performance.

⁸<https://huggingface.co/Qwen/Qwen3-Coder-30B-A3B-Instruct>

⁹<https://huggingface.co/Qwen/Qwen2.5-Coder-32B-Instruct>

Table 7. Comparison of Bug Rates w/ and w/o Error Correction Module.

	w/ Error Correction	w/o Error Correction
Bug Counts @ First 20 Iterations	3.51	4.73
Bug Counts @ Last 20 Iterations	2.67	3.92

Table 8. Performance with and without the Verification Agent on the Influenza-USA dataset.

	Mode	w/ Verification	w/o Verification
Influenza-USA	Mechanistic	4.81 \pm 1.50	8.46 \pm 1.82
	Hybrid	21.82 \pm 8.34	19.25 \pm 6.27

F. Prompts

F.1. Insights Extraction Prompt

Insights Extraction Prompt

I am trying to build a mechanistic epidemic model that can simulate transmission dynamics and generate forecasting predictions for daily infection counts. Please read and analyze the dataset I provide, identify important structural patterns, temporal behaviors, and feature relationships, and then generate actionable modeling tips specific to how a model should be designed, parameterized, or modified to fit this dataset well. Your tips may include suggestions on compartments, calibration strategies, seasonality, delays, under-reporting adjustment, spatial effects, or any dataset-specific phenomena you observe.

##Data

{string_data}

Please generate your tips after the ###TIPs:

E.g.,

###TIPs

Observation 1. [Your Observation 1 Here]

Tip 1. [Your Tip 1 Here]

Observation 2. [Your Observation 2 Here]

Tip 2. [Your Tip 2 Here] ...

F.2. Verification Prompt

Verification Prompt

Convert the following code into differential equations and assess whether the equations are physically grounded (e.g., non-negative compartments, conservation where appropriate, realistic rates). Keep reasoning concise.

Description:

{code_description}

Code:

“python

{state_code}

““

Checks: 1) ODE correctness: - Derive explicit equations for each state and parameter.

2) Physical validity:

- Non-negative compartments.
- Conservation holds when appropriate.
- Rates have valid signs and plausible roles.
- No undefined dynamics (e.g., division by zero).

3) Semantic consistency:

- States match the described compartments.
- Flow directions align with meaning (e.g., recovery $I \rightarrow R$).
- No missing or extra mechanisms relative to the description. - Parameters are used in their intended roles (e.g., β infection, γ recovery).
- Observed vs latent states are not conflated.
- Neural outputs (if any) are constrained and used consistently.

F.3. Reflection Prompt

Reflection Prompt

You generated the following code completions (ParamNN feeds a simulator; only ParamNN is trainable). Analyze them rigorously to drive the validation loss (RMSE) below {self.config.run.target_loss}.
 Records of the program after each iteration:““
 {history_best_completions_str} ““
 Current top programs (lowest validation loss last):““
 {completions} ““
 {error_section}
 Reflect step-by-step: 1. Diagnose weaknesses: For each program, explain why its validation loss (RMSE) isn't yet {self.config.run.target_loss} (look at structural choices, stability issues, etc.). If it is closed to the target, you should also identify which features have contributed to the success.
 2. Propose new designs: propose possible strategies that might drive the model to achieve lower validation loss.
 3. Repair plan: Propose specific code-level changes that address those root causes, including adjustments to ParamNN outputs, simulator couplings, or optimization targets. The plan must be actionable (e.g., “replace the quadratic interaction in line X with ... so the chemo input matches the observed decay”).
 4. Error handling (if present): For each failure listed above, pinpoint the bug and outline how to rewrite the affected section so it runs successfully next iteration.
 - Do not write full code; give concise, prescriptive instructions tied to the observed data. This reflection will guide generation {iteration} of {self.config.run.generations}.

F.4. Error Correction Prompt

Error Correction Prompt

Summarize code execution failures into concise bullets with key code fragments, error messages, and actionable fixes.
 Condense the repeated failures below. For each, keep a short code excerpt, the core error message, and a specific fix. {errors_text}
 The following section record generations that failed to run in the history. Reflect on the error messages also and describe how to fix the corresponding code so it executes correctly:
 #####
 {joined_errors}
 #####

F.5. Skeleton Codes Prompt

The skeleton codes are very similar across different datasets. Here we use Influenza-USA as an example.

```
class StateDifferential:
    def __init__(self, population, theta):
        # This section provides prefilled
        # code that enables the model to
        # incorporate meta-population
        # dynamics.
        # Initialize the parameters
        self.device = 'cuda:0'

        # migration matrix defines a matrix
        # describing the contact
        # probability among N locations.
        # Its size is (N, N)
        self.migration_matrix = theta

        # num_agents defines a vector
        # describing the population of
        # each location. Its size is (N)
        self.num_agents = population

        # self.num_patches is N.
        self.num_patches = self.
            migration_matrix.shape[0]

    def step(self, params, T):
        # TODO: Fill in the code here
        # You can use any number of
        # parameters from ['beta', 'kappa
        # ', 'symprob', 'epsilon', 'alpha
        # ', 'gamma', 'delta', 'mor'] to
        # construct the mechanistic model
        .
        # The shape of `params`: (self.
        # num_patches, T, 8)
        # Note that 'beta_t', 'kappa_t', '
        # symprob_t', 'epsilon_t', '
        # alpha_t', 'gamma_t', 'delta_t',
        # and 'mor_t' are all of shape (
```

```

self.num_patches)
# **You MUST NOT using any sub
loops except inside this loop
**
for t in range(T):
    (
        beta_t,
        alpha_t,
        gamma_t,
        delta_t,
        kappa_t,
        epsilon_t,
        symprob_t,
        mor_t,
    ) = params[:, t, :].unbind(dim
=-1)
S_t = S[-1]
E_t = E[-1]
I_t = I[-1]
R_t = R[-1]
M_t = M[-1]

# TODO: Fill in the code here
# - Remember this is a
deterministic ODE Simulator
# - Return 'I' as tensors,
where 'I' denotes the
simulated infected counts
along different time stamps
; 'I' should be the shape
of ('T'+1, self.num_patches
); params have a grad_fn,
so make sure that 'I' also
remains in the computation
graph.

return I

```

Note that the ‘population’ and the ‘theta’ are two constant vectors passed by the environment. We used the ones collected from a popular source¹⁰.

G. Qualitative Analysis on the Generated Mechanistic Codes

G.1. Semantically Wrong Codes

The model allows exposed individuals to transition to the removed state through two independent pathways:

$$E \xrightarrow{\alpha_t} R, \quad E \xrightarrow{\kappa_t(1-\text{symprob}_t)} R,$$

while only a fraction $\kappa_t \text{symprob}_t$ of exposed individuals become infectious. This makes the compartment E a non-identifiable reservoir whose outflow is governed by multiple unrelated rates.

```
def step(self, params, seed_status, T):
```

¹⁰<https://github.com/NSSAC/patchflow-data/tree/main>

```

kappa0 = params[:, 0, 4].clamp(0.01,
1.0)
symprob0 = params[:, 0, 6].clamp(0.01,
1.0)
I0 = (kappa0 * symprob0 * seed_status).
clamp(min=0.0)
E0 = (seed_status - I0).clamp(min=0.0)
S0 = (self.num_agents - E0 - I0).clamp(
min=0.0)
R0 = torch.zeros_like(seed_status)
M0 = torch.zeros_like(seed_status)
S = [S0]; E = [E0]; I = [I0]; R = [R0];
M = [M0]

for t in range(T):
    (beta_t, alpha_t, gamma_t, delta_t,
kappa_t, epsilon_t, symprob_t,
mor_t) = params[:, t, :].
unbind(dim=-1)

new_inf = (lambda_t * S_t).clamp(
min=0.0)
imp_inf = epsilon_t

dS = -new_inf
dE = new_inf - kappa_t * E_t +
imp_inf
dI = kappa_t * symprob_t * E_t - (
gamma_t + delta_t + mor_t) *
I_t
dR = gamma_t * I_t + alpha_t * E_t
+ kappa_t * (1 - symprob_t) *
E_t
dM = mor_t * I_t

```

Here is the second semantically incorrect mechanistic model. The error mainly comes from the fact that M_{next} variable is not updated consistently in the system.

```

S_next = S_t + dS
E_next = E_t + dE
I_next = I_t + dI
R_next = R_t + dR
M_next = M_t + dM

S_next = torch.clamp(S_next, min=0)
E_next = torch.clamp(E_next, min=0)
I_next = torch.clamp(I_next, min=0)
R_next = torch.clamp(R_next, min=0)
M_next = torch.clamp(M_next, min=0)

alive_sum = S_next + E_next + I_next +
R_next
total = alive_sum + M_next
excess = torch.clamp(total - self.
num_agents, min=0)

if torch.any(excess > 0):
    nonM = alive_sum + 1e-8
    fracS = S_next / nonM
    fracE = E_next / nonM
    fracI = I_next / nonM
    fracR = R_next / nonM

```

```
S_next = S_next - fracS * excess
E_next = E_next - fracE * excess
I_next = I_next - fracI * excess
R_next = R_next - fracR * excess
# M_next (cumulative deaths) is left
  untouched
```

Here is the third semantically incorrect mechanistic model. A parameter δ_t intended to represent a rate is injected as an absolute flow, creating a unit mismatch and breaking mechanistic interpretability

```
dS = -new_exposed + alpha_t * R_t
dE = new_exposed - kappa_t * E_t + delta_t
dI = kappa_t * E_t - gamma_t * I_t - mor_t
  * I_t
dR = gamma_t * I_t - alpha_t * R_t
dM = mor_t * I_t
```

```
class StateDifferential:
  def step(self, params, seed_status, T):
    ...

    # Clamp for biological plausibility
    S_next = torch.clamp(S_t + dS, min
      =0.0, max=self.num_agents)
    E_next = torch.clamp(E_t + dE, min
      =0.0, max=self.num_agents)
    I_next = torch.clamp(I_t + dI, min
      =0.0, max=self.num_agents)
    R_next = torch.clamp(R_t + dR, min
      =0.0, max=self.num_agents)
    M_next = torch.clamp(M_t + dM, min
      =0.0, max=self.num_agents)

    ...
  return I
```

G.2. Run-time Error Codes

The following snippets present examples of generated code that yield runtime errors.

Indentation Error The code line `dS=-lambda_t * S_t` has a wrong indentation, leading to the indentation error.

```
Error: Error running function: File "<string>", line 74
      dE = lambda_t * S_t - kappa_t *
        E_t
      ^
IndentationError: unexpected indent

```python
...
dS = -lambda_t * S_t
 dE = lambda_t * S_t - kappa_t * E_t
 dI = kappa_t * E_t - (gamma_t +
 delta_t + mor_t) * I_t
 ...
 return I
```
```

Function Error When calling the function `clamp()`, wrong parameter types are provided.

```
Error: Error running function:
  TypeError: clamp() received an
  invalid combination of arguments -
  got (Tensor, max=Tensor, min=float)
  , but expected one of:
  * (Tensor input, Tensor min = None, Tensor
    max = None, *, Tensor out = None)
  * (Tensor input, Number min = None, Number
    max = None, *, Tensor out = None)

```python
import torch
```

### G.3. Evolving Code Examples

The table 9 shows a summarization about what changes have been made to the generated model across different iterations in a typical run.

Table 9. Evolution of Mechanistic Model Design and Validation Loss for the Influenza-USA dataset

Phase / Iteration Range	Structural Change	Val. Loss	Loss Change ( $\Delta$ )	Main Contribution
Iteration 0 (Baseline)	Basic SEIRM, Euler update, no clamping, prevalence output	$\sim 28.1$	–	Numerically unstable, mismatch with reported flu data, unconstrained parameters
Iteration 1	Explicit $dt$ , state clamping, death compartment, improved $\kappa$ usage	$\sim 24.8$	–3.3	Stabilized dynamics and transmission scaling
Early–Mid (Iter $\sim 10$ –20)	Mass conservation, partial switch to incidence output	$\sim 15.36$	–9.4	Prevented population drift; incidence aligns better with surveillance data
Mid–Late (Iter $\sim 20$ –28)	Inconsistent designs, partial smoothing/reporting logic	$\sim 15$ –20	$\approx 0$ to +5	Over-complication sometimes hurt generalization
Iteration 31	Learnable init split, reporting rate, background/import, smoothing kernel	$\sim 17.19$	–	First explicit observation model
Iteration 32 (Break-through)	Constrained params (soft-plus/sigmoid), nonlinear FOI, learnable smoothing, reported incidence output	$\sim 5.86$	–9 to –11	Matched data type, noise structure, and stabilized optimization